Available online at www.sciencedirect.com
ScienceDirect
Journal of Power Sources 161 (2006) 1106–1115
JOURNAL OF POWER SOURCES
www.elsevier.com/locate/jpowsour

Direct measurement of through-plane thermal conductivity and contact resistance in fuel cell materials

Manish Khandelwal, M.M. Mench *

Fuel Cell Dynamics and Diagnostics Laboratory, Department of Mechanical and Nuclear Engineering, The Pennsylvania State University, University Park, PA 16802, United states

Received 18 April 2006; received in revised form 24 May 2006; accepted 6 June 2006
Available online 17 August 2006

Abstract

An experimental study to determine the through-plane thermal conductivity of dry Nafion®, various diffusion media, catalyst layer, and the thermal contact resistance between diffusion media and a metal plate as a function of temperature and pressure was performed. Dry Nafion® thermal conductivity was determined to be $0.16 \pm 0.03\ W\ m^{-1}\ K^{-1}$ at room temperature, which decreases to $0.13 \pm 0.02\ W\ m^{-1}\ K^{-1}$ at 65 °C. Diffusion media thermal conductivity was found to be function of PTFE content and manufacturer, and was $0.48 \pm 0.09\ W\ m^{-1}\ K^{-1}$ for untreated and $0.22 \pm 0.04\ W\ m^{-1}\ K^{-1}$ for 20 wt.% PTFE treated SIGRACET® diffusion media, respectively. Toray diffusion media thermal conductivity was measured to be $1.80 \pm 0.27\ W\ m^{-1}\ K^{-1}$ at 26 °C and decreases to $1.24 \pm 0.19\ W\ m^{-1}\ K$ at 73 °C. The thermal contact resistance between Toray carbon paper and aluminium bronze material was determined to vary from 6.7×10^{-4} to $2.0 \times 10^{-4}\ m^2\ K\ W^{-1}$ for an increase in compression pressure from 0.4 to 2.2 MPa. The equivalent thermal conductivity of a 0.5 mg cm^{-2} platinum loaded catalyst layer was estimated to be $0.27 \pm 0.05\ W\ m^{-1}\ K^{-1}$. A one-dimensional analytical model was also used to estimate the temperature drop in the fuel cell components. A maximum of 3–4 °C temperature drop can be expected for a 200 μm thick SIGRACET® diffusion media at 1 A cm^{-2}. The thermal properties characterized should be useful to help modelers accurately predict the temperature distribution in a fuel cell.

Keywords: Thermal conductivity; Fuel cells; Nafion® membrane; Diffusion media; Thermal contact resistance

1. Introduction

Detailed knowledge of the internal temperature distribution in a polymer electrolyte fuel cell (PEFC) is critical for efficient water and thermal management. In a fuel cell, local variation in temperature can be attributed to the waste heat generation, which includes the irreversible heat of electrochemical reaction, losses due to over-potential at each electrode and Joule heating in all components, but mostly the electrolyte. The temperature distribution can affect the drying/flooding and degradation phenomenon in the fuel cell, which deteriorates its performance. Therefore, a thorough knowledge of *in situ* temperature distribution is essential for understanding the thermal and water transport in a PEFC.

Direct *in situ* temperature measurement introduces additional challenges due to the minute length scale involved, anisotropic nature of porous media, and existence of complex two-phase flow in the PEFC. Various modeling approaches [1–4] have been presented to predict the temperature distribution of PEFC under different operating conditions. However, limited information available in the literature on the varying through-plane and interfacial thermal resistance values of fuel cell components presents a barrier for the modelers. Highly accurate estimation of temperature distribution is impossible without complete knowledge of the cell component's thermal properties under different operating conditions, PTFE content, and compression.

Several studies have been performed by various researchers to determine the thermal conductivity of various materials for non fuel cell applications. Washo and Hansen [5] used the steady state method to measure thermal conductivity of oriented, amorphous specimens of polymethylmethacrylate (PMMA) and polystyrene. In the field of micro-electro-mechanical system (MEMS), numerous studies have been performed to determine the thermal property of thin films and polymers [6–15]. Kurabayashi et al. [8] have used steady state Joule heating and harmonic Joule heating method with electrical thermom-

* Corresponding author. Tel.: +1 814 865 0060; fax: +1 814 863 4848.
E-mail address: mmm124@psu.edu (M.M. Mench).

0378-7753/$ – see front matter © 2006 Elsevier B.V. All rights reserved.
doi:10.1016/j.jpowsour.2006.06.092

etry resistance (or optical thermometry [9]), to measure the in-plane and through-plane thermal conductivity of spin-coated polyimide films. Choy et al. [10,11,16] have developed a flash radiometry technique to determine the thermal conductivity (thermal diffusivity) of polymer films. Kurabayashi [6] have presented a brief review of various experimental and mathematical models for measurement of thermal conductivity in the in-plane and through-plane directions for various polymers. A guarded heat flow meter (using ASTM E1530 procedure) was used by Song et al. [17,18] to measure thermal conductivity of lithium polymer electrolyte and composite cathode for lithium batteries. Morotta and co-workers [19,20] also studied the thermal conductivity and thermal contact resistance of various thermoplastic and thermosetting polymers using the flux measurement. A detailed review is presented by Savija et al. [21] on various analytical and experimental methods for thermal contact resistance.

To the author's knowledge, none of the above methods for thin films have been used for determination of thermal conductivity of fuel cell materials. Vie and Kjelstrup [22] estimated thermal conductivity of a fuel cell membrane by measuring *in situ* temperature gradients in a fuel cell. Burford and Mench [23] also estimated thermal conductivity of diffusion media and Nafion® by measuring electrolyte temperature using microthermocouples embedded in the electrolyte. Non-isothermal and two-phase modeling literature [1–3,24,25] has used inconsistent thermal conductivity values for PEFC materials. Table 1 summarizes the thermal conductivity values of fuel cell material reported in the literature by various researchers. Unfortunately, limited experimental data are available for thermal conductivity and contact resistance of PEFC material to support the mathematical models. This work is meant to provide reliable bench mark data for modelers to accurately predict the temperature distribution in a fuel cell. In this paper, an experimental technique based on a steady state measurement method [19,26] is used to accurately measure the thermal conductivity of dry Nafion® membrane, diffusion media (DM) with different PTFE content, and from various manufacturers, a catalyst layer, and the contact resistance between the diffusion media and metal plate as function of temperature and/or compression pressure. Care was taken to provide accurate assessment of the experimental uncertainty.

Table 1
Thermal conductivity (W m^{-1} K^{-1}) of fuel cell components reported by various authors in the literature

	Diffusion media	Catalyst layer	Membrane	Author/reference
1	0.5, 1.0, 2.94[a]	–	0.95[a]	Ju et al. [1]
2	–	–	0.67[a]	Berning et al. [2]
3	1.7[a]	–	0.5[a]	Hwang [3]
4	–	–	0.1 ± 0.1[b]	Vie and Kjelstrup [22]
5	0.13–0.19[b]	–	0.025–0.25[b]	Burford and Mench [23]
6	1.5[a]	1.6[a]	0.34[a]	Rowe and Li [24]
7	0.15[a]	0.2[a]	0.21[a]	Argyropoulos et al. [25]

[a] Estimated value.
[b] Experimentally measured value.

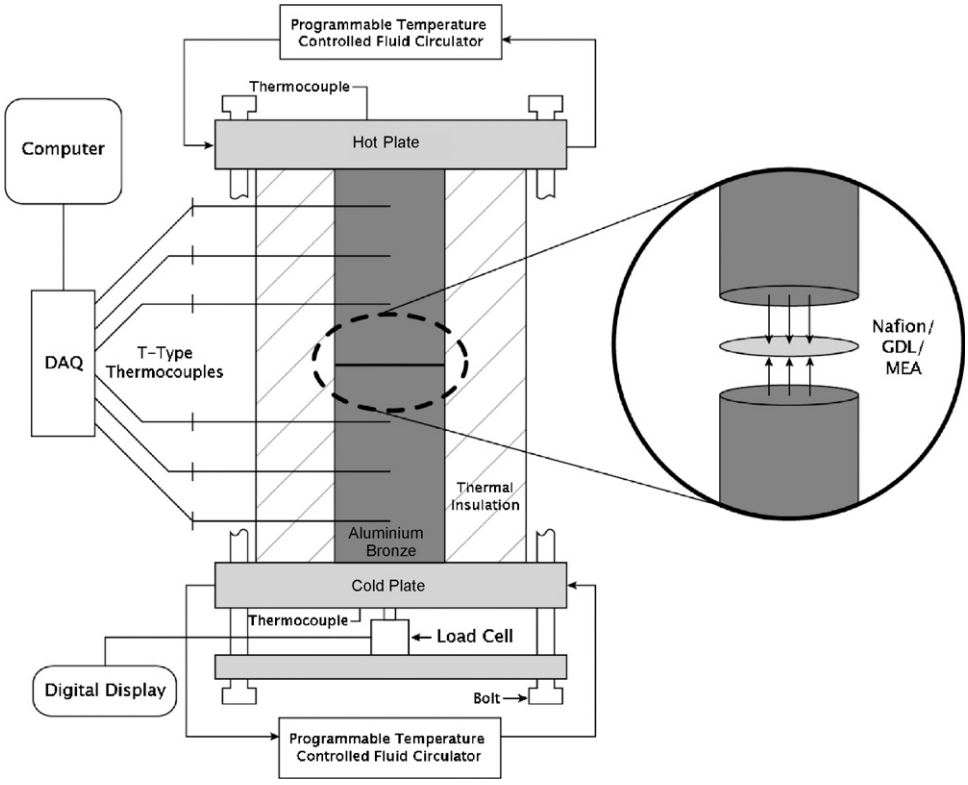

Fig. 1. Schematic diagram of the test setup to measure thermal conductivity and thermal contact resistance of thin films.

2. Experimental setup

The schematic diagram of the test rig for the thermal contact resistance and through-plane thermal conductivity measurement of thin films is shown in Fig. 1. In this configuration, an insulated long circular cross section of standard material with known thermal conductivity is uniformly compressed between two backing plates. Both backing plates are maintained at a different constant temperature, thus acting as a heat source and sink, to generate the heat flow. Thermocouple arrays are inserted in the cylindrical standard material above and below the test sample. The test sample with unknown thermal conductivity is placed between the two standard material cylinder rods. The compression pressure is precisely controlled and measured with a load cell.

2.1. Design and instrumentation

The test setup was designed based on two criteria. First is to achieve nearly one-dimensional heat transfer in the axial direction. And second was to achieve a temperature drop in adjacent thermocouple locations that is comparable in magnitude to the temperature drop across the test specimen, so that the signal to noise ratio is maximized. Comprehensive design and analysis were performed to select the standard material based on its thermal conductivity, to determine the assembly dimensions and thickness of the insulation. Based on this analysis, aluminum bronze (C613, $k = 54.5\ \mathrm{W\,m^{-1}\,K^{-1}}$) was chosen as the standard material above and below the specimen. The test specimen was placed between two cylindrical pieces of standard material 7.62 cm (3 in.) in length and 5.08 cm (2 in.) in diameter. Three high precision thermocouples (TMQSS-125-G-6, Omega Engineering) per array were fixed equidistantly in the upper and lower pieces of the standard material. The temperatures of upper and lower compression plates were monitored by a T-type fast response self-adhesive thermocouple (SA1-T, Omega Engineering). A load cell (LC304-1K, Omega Engineering) was placed between the two bottom plates to measure the compression pressure. To limit radial heat leakage, thermal insulation was provided by several layers of polyethylene foam wrap around the standard material/specimen. The steady upper and lower plate temperatures were maintained by passing high flow rate coolant fluid through channels inside the plates from an insulated programmable temperature controller baths (VWR 1157P). During experimentation, the entire system was monitored at a specified condition for 8–10 h to ensure a true steady state. Steady state was assumed to be reached when the temperature fluctuation in each measured point in the system was less than 0.5 °C in 30 min.

2.2. Measurement and uncertainty analysis

At steady state, the temperature at each location in the upper and lower thermocouple arrays was measured and averaged over a time span of 20–30 min for the analysis. The results were linearly extrapolated to the test specimen edge, to determine the temperature drop across the test specimen. Fig. 2 shows a plot for an experiment with 127 μm (0.005 in.) polyethylene film as the test specimen. With the knowledge of standard material thermal conductivity, the precise heat flux across the specimen can be calculated using Fourier's law [27] in the axial direction. Since the heat flux is proportional to the temperature difference, the through-plane thermal resistance across the thin film test specimen can be easily determined. This measurement includes the thermal resistance provided by test specimen and thermal contact resistance between test specimen and standard material. By performing the experiment with two different thickness of test specimen, the intrinsic thermal conductivity (thermal resistance of specimen) and thermal contact resistance between the specimens can be determined at the measured compression pressure and temperature.

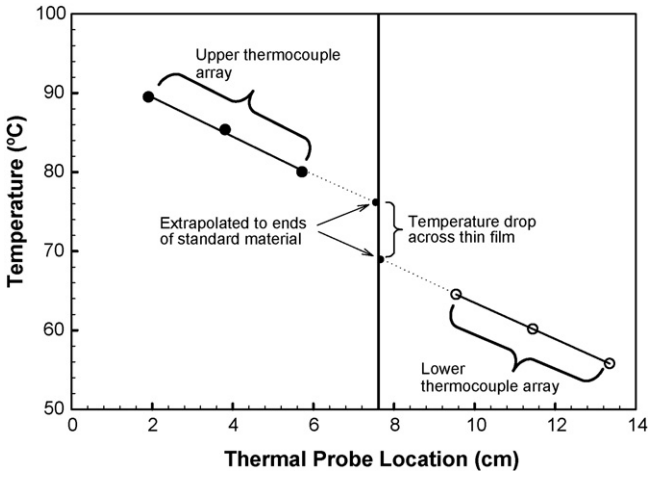

Fig. 2. Steady state temperature profile at thermal probe location for validation experiment with 127 μm (0.005 in.) thick polyethylene sample (vertical line shows the location of thin film).

The thermal contact resistance between two surfaces is a function of pressure and surface roughness [27]. The test system allows for the investigation of effect of pressure on thermal contact resistance. Surface roughness effects were minimized in the design by using polished metal contact surfaces. A digital display connected with the load cell allows the applied load to be determined. The effect of temperature on the intrinsic through-plane thermal conductivity was studied by varying the heat flow through the test specimen. This was achieved by altering the temperature set points of the end plates. Temperature controllers can provide set point temperature from −15 to 120 °C. This constrained along-with the second design criteria provides a minimum and maximum average temperature of 10–15 and 60–70 °C for the test specimen, respectively.

The test system was designed to minimize the uncertainty in the experiment. Heat loss in the radial direction and the thermocouple measurement are considered to be the major potential sources of uncertainty. Uncertainty in temperature measurement is accounted for probe placement in the hole [28] and its tolerance. Uncertainty in the specimen dimension is accounted for the manufacturing tolerance. A detailed uncertainty analysis was conducted according to the method described by Kline and McClintock [29]. This method allows estimation of the uncertainty of experimental measurements. If a given variable G is a function of several variables so that $G = G(x_1, x_2, \ldots, x_n)$, then

the uncertainty in G, providing uncertainties in x_1–x_n are not coupled, is shown as

$$u_G = \sqrt{\left[\left(\frac{\partial G}{\partial x_1}u_1\right)^2 + \left(\frac{\partial G}{\partial x_2}u_2\right)^2 + \cdots + \left(\frac{\partial G}{\partial x_n}u_n\right)^2\right]} \quad (1)$$

where u_G is the uncertainty of variable G, and u_1–u_n are the uncertainties of variable x_1–x_n, respectively. For the thermal conductivity of specimen, all dimensions and thermal conductivity of standard material, specimen thickness, and temperature measurement were considered as the dependent variables. Based on this analysis, the estimated uncertainty in the thermal resistance (thermal conductivity) of the specimens should be less than 15% of measured value, with most uncertainty as a result of radial heat leak. With the current design and dimensions, the estimated ratio of radial and axial flux should be less than 10%.

3. Result and discussion

3.1. Measurement technique validation

The test system and measurement technique was validated with both metal and thin films. Aluminum bronze (same as the standard material) samples of thickness 2.54 cm (1 in.) and 5.08 cm (2 in.) were used to validate the measurement technique. The thermal conductivity measured was 8% higher than the actual value, which is within the expected experimental uncertainty and is likely the result of some radial heat leak. Polyethylene films of thickness 127 μm (0.005 in.), 254 μm (0.010 in.) and 508 μm (0.020 in.) were used to validate the test setup for thin films. The calculated thermal conductivity for the polyethylene film was estimated $0.35 \pm 0.05\,\mathrm{W\,m^{-1}\,K^{-1}}$. The measured value is 10% higher than the reported value in the literature $0.32\,\mathrm{W\,m^{-1}\,K^{-1}}$ [11,30], and lies within the calculated measurement uncertainty. An overestimation of the actual thermal conductivity is expected, due to the radial heat loss. However, since the exact radial heat loss varies between cases, it cannot be arbitrarily adjusted to correct in the thermal conductivity value. Nevertheless, it is expected that all values reported here are 5–10% higher than the actual values because of this effect. Results of a steady state temperature profile for the validation experiment for a 127 μm (0.005 in.) thin polyethylene sample are shown in Fig. 2. The experimentally measured thermal conductivities of various commonly used fuel cell components is summarized in Table 2, and discussed in the following sections.

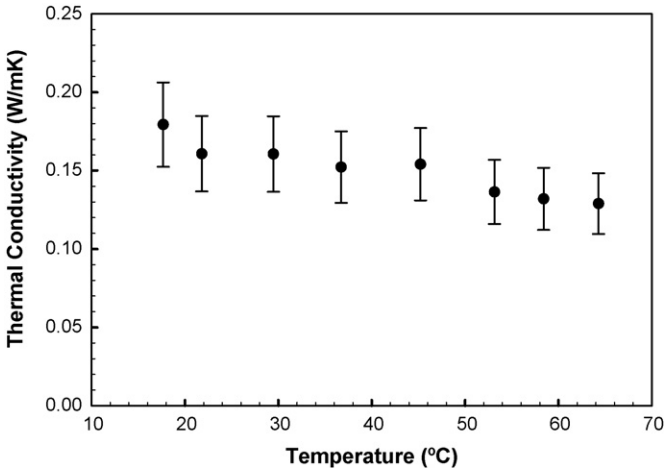

Fig. 3. Measured thermal conductivity as a function of temperature for dry Nafion® membrane (using Nafion® 112 and Nafion® 117), error bar calculated at 15%.

Repeatability of measurement is estimated to be 15–20% based on repeated test on Nafion® membrane at high compression pressure (~2 MPa). However, additional variation can be expected at reduced compression pressure due to non-uniform contact.

3.2. Nafion® membrane

The thermal conductivity of DuPont Nafion® membrane (provided by IonPower Inc.) over a range of temperatures from 17 to 65 °C is plotted in Fig. 3. To estimate dry Nafion® thermal conductivity (at atmospheric condition), Nafion® 112 and Nafion® 117 samples were tested as delivered, with no external humidification. At room temperature, dry Nafion® thermal conductivity was found to be $0.16 \pm 0.03\,\mathrm{W\,m^{-1}\,K^{-1}}$. At the highest measured temperature of 65 °C, the thermal conductivity of Nafion® was determined to be $0.13 \pm 0.02\,\mathrm{W\,m^{-1}\,K^{-1}}$. At 80 °C, the thermal conductivity can be linearly extrapolated as $0.11 \pm 0.02\,\mathrm{W\,m^{-1}\,K^{-1}}$. The measured thermal conductivity

Table 2
Experimentally measured thermal conductivity of PEFC components

Material	Measured thermal conductivity, k ($\mathrm{W\,m^{-1}\,K^{-1}}$)	Reported/estimated value in literature ($\mathrm{W\,m^{-1}\,K^{-1}}$)
DuPont Nafion® membrane (at 30 °C)	0.16 ± 0.03	0.1–0.95
Toray carbon fiber paper diffusion media (TGP-H-60 at 26 °C)	1.80 ± 0.27	1.7 [37]
SIGRACET® 0 wt.% PTFE carbon-fiber paper diffusion media (AA series at 56 °C)	0.48 ± 0.09	Not available
SIGRACET® 5 wt.% PTFE carbon-fiber paper diffusion media (BA series at 58 °C)	0.31 ± 0.06	Not available
SIGRACET® 20 wt.% PTFE carbon-fiber paper diffusion media (DA series 58 °C)	0.22 ± 0.04	Not available
E-Tek ELAT® diffusion media (LT1200-W at 33 °C)	0.22[a] ± 0.04	Not available
Catalyst layer (0.5 mg cm^{-2} platinum on carbon)	0.27[b] ± 0.05	Not available

[a] Thermal conductivity based on single and double layer of diffusion media as test specimen (neglecting contact resistance between the two layers of diffusion media).
[b] Effective thermal conductivity (includes thermal contact resistance with diffusion media).

is in good agreement with the experimental observation of Vie and Kjelstrup [22], and Burford and Mench [23] as shown in Table 1.

It was observed that the thermal conductivity of Nafion® decreases with increasing temperature, where the test temperature is defined as the average temperature across the test specimen. Although the downward trend in thermal conductivity is nearly within the error bar limit, this behavior of Nafion® may be explained on the basis of its structure and morphology. Kenneth and Moore [31], and other researchers [32,33] have presented a comprehensive review on the fundamental structure and properties of Nafion® perfluoronate materials and its applications. Using small angle X-ray scattering (SAXS) and wide angle X-ray diffraction (WAXD), Gierke and co-workers [34,35] also examined and compared morphological features of Nafion® and attributed these features to a crystalline structure within the fluorocarbon matrix. For a crystalline polymer, Choy et al. [11,36] has explained an inverse relation between temperature and thermal conductivity based on the phonon transport. They reported that the thermal conductivity, k, of an insulating material is given as [11,18]:

$$k = \frac{1}{3}cvl \tag{2}$$

where c is the phonon heat capacity, v the phonon velocity and l is the phonon mean free path. The collision probability of phonons increases at high temperature due to an increase in the number of participating phonons. Consequently, the mean free path l decreases, while the c and v remain almost constant. Thus, the thermal conductivity, which is proportional to the mean free path, decreases with an increase in the temperature for a crystalline insulating material, such as Nafion®.

The effect of humidity on the thermal conductivity of the Nafion® membrane can be theoretically estimated by assuming the humidified membrane as mixture of water and dry membrane. Using volume averaging, the thermal conductivity of a humidified membrane can be estimated as

$$\bar{k} = \frac{(\lambda_w/\rho_w)k_w + (1/c_{SO_3^-}M_w)k_{nf}}{1/c_{SO_3^-}M_w + \lambda_w/\rho_w} \tag{3}$$

where λ_w is the water content in Nafion® (mol H_2O/mol SO_3^{-1}), ρ_w the density of water (kg m^{-3}), k_w the thermal conductivity of water (W m^{-1} K^{-1}), M_w the molecular weight of water (kg kmol^{-1}), $c_{SO_3^-}$ the molar concentration of SO_3^- ion (mol l^{-1}) and k_{nf} is the thermal conductivity of dry Nafion® membrane (W m^{-1} K^{-1}). Note that the non-homogenous water distribution in the membrane may cause error in this estimation. Nevertheless, it serves to bound the expected thermal conductivity of a humidified membrane for calculation and comparison purposes. From Eq. (3), the estimated variation of thermal conductivity of humidified Nafion® membrane with temperature was calculated, and is shown in Fig. 4 for different humidity ratios. For a fully humidified membrane, the thermal conductivity was estimated to be 0.29 ± 0.03 W m^{-1} K^{-1} at 65 °C. It is important to observe that water thermal conductivity increases with temperature; however the inverse relation is true for dry Nafion®. Hence, for the case of 80% or fully humidified condition (100%), the membrane thermal conductivity is uniform with temperature within the experiment tolerance. The thermal conductivity of pure liquid water is shown in Fig. 4 as an upper bound on the maximum possible thermal conductivity.

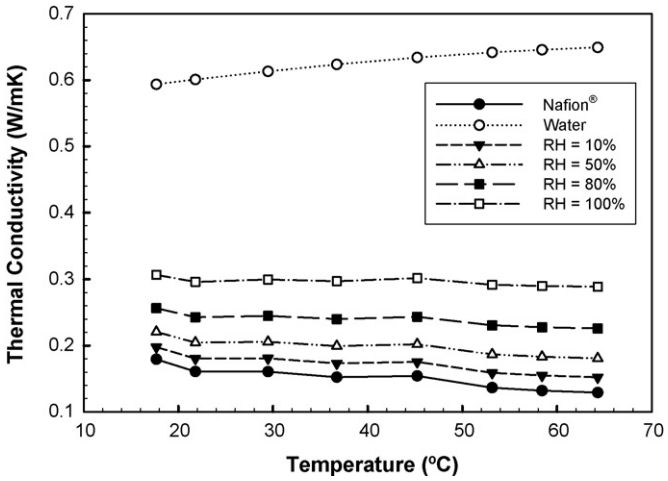

Fig. 4. Estimated thermal conductivity of Nafion® 1100 EW at different humidity ratios. The thermal conductivity variation of pure water is shown as an upper bound for the theoretical moist Nafion® thermal conductivity.

3.3. Diffusion media

Toray carbon paper "TGP-H" [37] (0 wt.% PTFE) diffusion media were investigated to measure the thermal conductivity and thermal contact resistance with the aluminum bronze standard material under various temperature and compression pressures. Two diffusion media samples with thickness of 190 μm (TGP-H-60, 78% porosity) and 280 μm (TGP-H-90, 78% porosity) were used in the experiment. The measured intrinsic material thermal conductivity at 26 °C was found to be 1.80 ± 0.27 W m^{-1} K^{-1}, which is in close agreement with the value provided in the specification of the material from the manufacturer of 1.70 W m^{-1} K^{-1} [37]. Variation of thermal conductivity of Toray carbon paper (TGP-H-60) with temperature is shown in Fig. 5 and it decreases from 1.80 ± 0.27 W m^{-1} K^{-1} at 26 °C to 1.24 ± 0.19 W m^{-1} K^{-1} at 73 °C. This inverse relation of thermal conductivity with temperature for carbon paper may be explained based on the presence of carbonized thermo setting resin [41], which acts as a binder in the diffusion media. Based on the phonon transport [11,18], thermal conductivity of these thermo-setting polymer decreases with increasing temperature. For diffusion media without any binder material, insignificant changes (±0.04 W m^{-1} K^{-1}) in thermal conductivity were observed for carbon cloth (ELAT® LT 1200-W) in the temperature range of 30–60 °C.

Variation of thermal contact resistance of Toray carbon paper with aluminum bronze material for different compression pressure was calculated and is shown in Fig. 6. In this experiment, the initial pressure was gradually increased from 0.4 to 2.2 MPa, and then reduced to 0.4 MPa. Hysteresis is observed due to diffusion media fiber compression and deformation. An asymp-

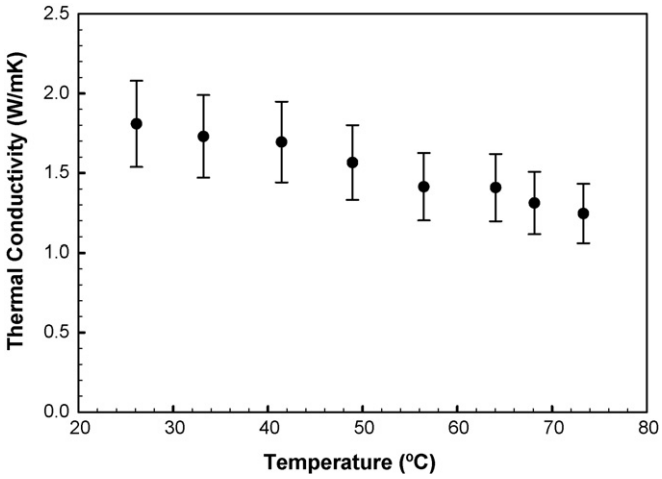

Fig. 5. Measured thermal conductivity as a function of temperature for Toray carbon paper (TGP-H-60), error bar calculated at 15%.

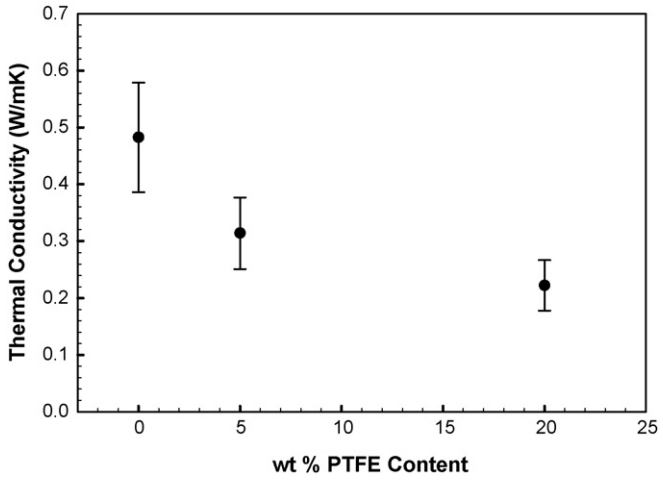

Fig. 7. Variation of thermal conductivity of the SIGRACET® diffusion media with wt.% PTFE content at 2 MPa compression pressure and 56–58 °C.

totic approach to a minimum value, corresponding to a fully compressed diffusion media surface, is seen near 2 MPa pressure ranges, which corresponds to a thermal contact resistance of 2.0×10^{-4} m^2 K W^{-1}. Contact resistance is also function of type of the material. So, the reported value here may differ from the contact resistance with graphite or other cell materials with different surface finish. The point is to show the hysteresis that exists as a function of compression pressure.

3.4. Effect of PTFE content on diffusion media thermal conductivity

To study the effect of hydrophobic additive polytetrafluoroethylene (PTFE) on the diffusion media thermal conductivity, experiments were performed on SIGRACET® AA (0 wt.% PTFE), BA (5 wt.% PTFE) and DA (20 wt.% PTFE) series diffusion media [38], with thicknesses of 190 and 280 μm. The variation of thermal conductivity with PTFE content for these SIGRACET® diffusion media is shown in Fig. 7. It was observed that thermal conductivity decreases with increasing PTFE content. For low PTFE content (5 wt.%), the thermal conductivity (0.31 ± 0.06 W m^{-1} K^{-1}) is reduced by 35% as compared to the untreated diffusion media (0.48 ± 0.09 W m^{-1} K^{-1}). However, with increase in weight percent of PTFE content from 5 to 20, the diffusion media thermal conductivity was further reduced only by 29% (0.22 ± 0.04 W m^{-1} K^{-1}). Therefore, with further increase in the weight percent of PTFE the thermal conductivity of PTFE treated diffusion media could approach an asymptotic value. The porosity value of all SIGRACET® diffusion media was 82–85%, implying some of the high thermal conductive carbon fibers ($k_{carbon} = 129$ W m^{-1} K^{-1} [39]) are coated by low thermally conducting PTFE material ($k_{PTFE} = 11.7$ W m^{-1} K^{-1} [40]). This could be attributed as one of the possible reasons for reduction in thermal conductivity of PTFE treated diffusion media. Scanning electron microscopy (SEM) images of PTFE treated and untreated SIGRACET® diffusion media are given in Fig. 8. Other work [41] has also identified the PTFE distribution preferentially near the diffusion media surface. Due to the coverage of these carbon fibers, the thermal resistance is increased, which leads to the reduction in the effective thermal conductivity of PTFE treated diffusion media. In theory, PTFE addition can actually increase the thermal conductivity of the DM if the PTFE displaces a significant amount of lower thermal conductive air. However, this was not the case. The thermal contact resistance was determined to be 1.3×10^{-4}, 1.5×10^{-4} and 1.2×10^{-4} m^2 K W^{-1} for SIGRACET® untreated, 5 and 20 wt.% PTFE content diffusion media, respectively at 2.2 MPa.

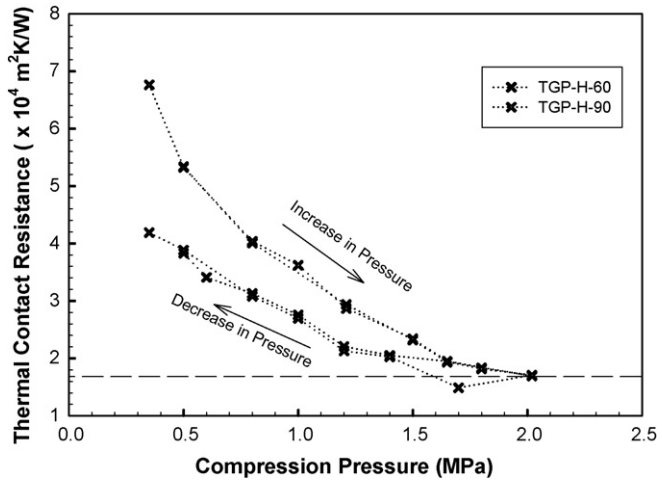

Fig. 6. Variation of thermal contact resistance between Toray carbon paper and smooth aluminum bronze with compression pressure, TGP-H-60 (0.19 mm thick) and TGP-H-90 (0.28 mm thick) with 78% porosity.

3.5. Catalyst layer

The catalyst layer which is a mixture of electrolyte and 0.5 mg cm^{-2} platinum powder loading supported by large carbon particles, was hot pressed on both sides of a polymer electrolyte membrane. This three-layer membrane structure is often referred as membrane electrode assembly (MEA). To determine the through-plane thermal resistance of the catalyst layer, experiments were performed on a MEA (Nafion® 112 membrane,

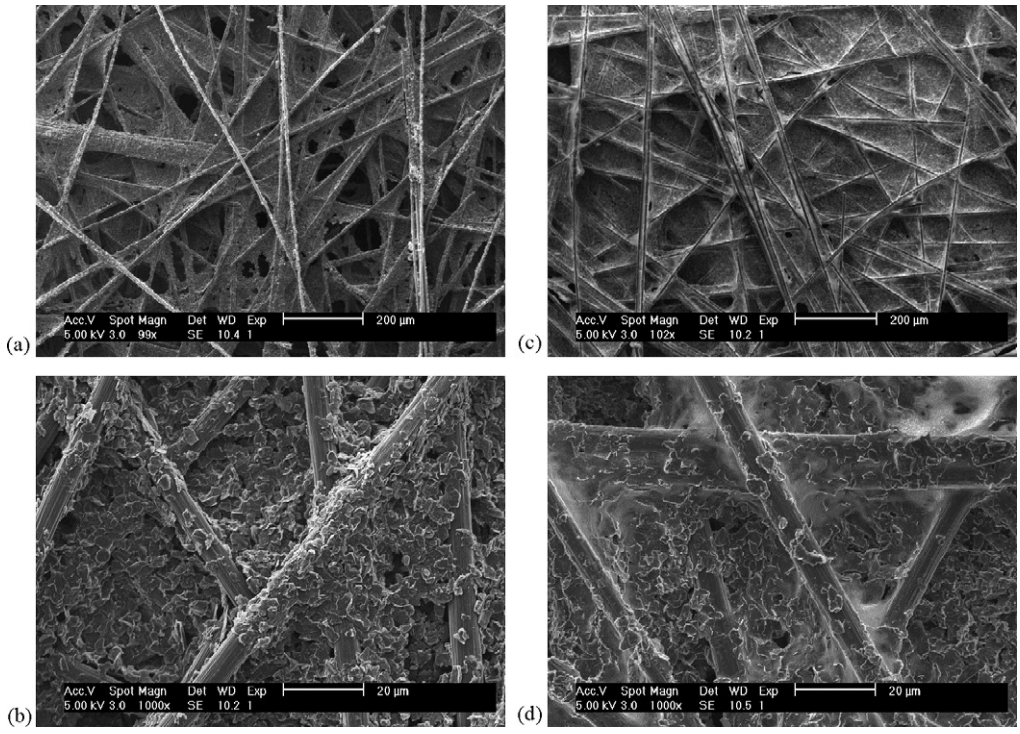

Fig. 8. Scanning electron microscopy (SEM) image of SIGRACET® PTFE treated and untreated diffusion media at different magnification: (a)–(b) untreated diffusion media (type 24 AA); (c)–(d) 20 wt.% PTFE diffusion media (type 24 DA).

cathode/anode catalyst layer: 25 μm, manufacturer: Lynntech, provided by FuelCellStore.com) having a diffusion media (Toray carbon paper: TGP-H-60) on both side. From previous experiments, the membrane thermal conductivity, diffusion media thermal conductivity and its contact resistance with the standard material are known. So, the combined thermal resistance of the catalyst layer and contact resistance with the diffusion media can be determined. This value was termed the effective thermal resistance of the catalyst layer. Variation of the effective thermal contact resistance with compression pressure for a catalyst layer is shown in Fig. 9. An asymptotic region is approached at compression pressure ~2 MPa which corresponds to thermal contact resistance $1 \times 10^{-4}\,\mathrm{m^2\,K\,W^{-1}}$. This thermal resistance value may be very helpful for non-isothermal mathematical models which presently ignore the catalyst layer contribution to the thermal resistance. The equivalent effective thermal conductivity of the catalyst layer was also estimated as $0.27 \pm 0.05\,\mathrm{W\,m^{-1}\,K^{-1}}$, which is similar in magnitude to that of the diffusion media.

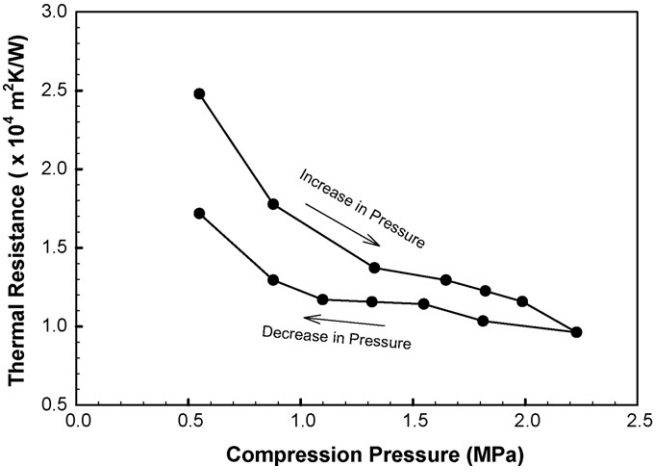

Fig. 9. Variation of effective thermal resistance (including thermal contact resistance with Toray carbon paper) of 0.5 mg cm^{-2} platinum loaded catalyst layer with compression pressure.

3.6. Theoretical study of temperature drop in a fuel cell

A simple analytical model based on one dimensional conduction heat transfer was developed to predict the typical temperature drop in the fuel cell components using the new thermal transport parameter. This one-dimensional approach is reasonable as a first approximation to investigate the effect of material properties on the temperature distribution in a fuel cell.

The simplified 1D model accounts for the heat transfer from the membrane, anode/cathode diffusion media, catalyst layer and backing plate, as shown in Fig. 10. Steady state is assumed and conduction heat transfer from the flow channel is neglected, since it is typically relatively small. The heat source is considered from Joule heating in the membrane. In the catalyst layers, the heat source is calculated from the respective half-cell reaction entropic loss, activation, concentration over-potential, and joule heating. The governing equation in each component can be written from the Fourier's law [27]:

$$k\frac{\partial^2 T}{\partial x^2} = q''' \tag{4}$$

where k is the thermal conductivity of the material ($\mathrm{W\,m^{-1}\,K^{-1}}$), T the temperature (K) and q''' ($\mathrm{W\,m^{-3}}$) is the volumetric heat

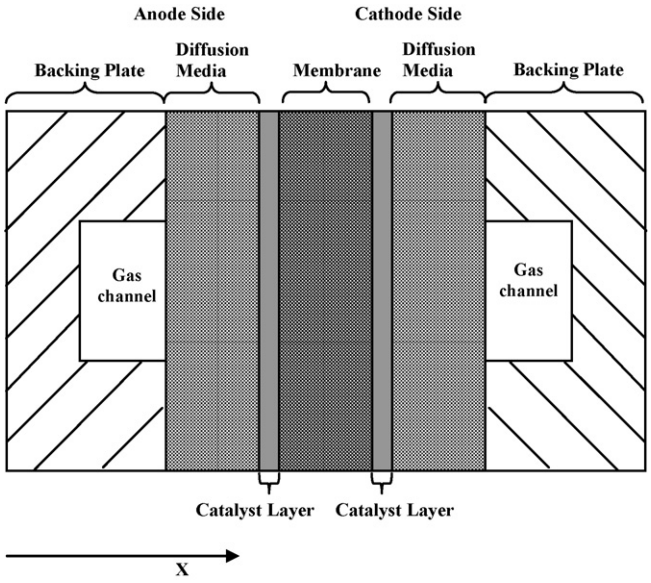

Fig. 10. Schematic of polymer electrolyte fuel cell for the simplified 1D analytical conduction model for thermal transport.

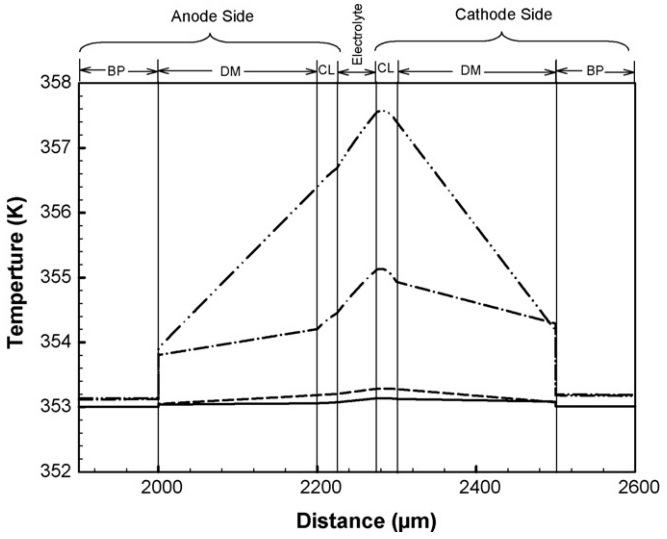

Fig. 11. Estimated temperature drop in fuel cell component for current density $i = 0.1$ and $1.0\ \mathrm{A\,cm^{-2}}$ for Toray carbon paper and SIGRACET® 5% PTFE as the diffusion media. (—) $i = 0.1\ \mathrm{A\,cm^{-2}}$ (Toray), (– · – · –) $i = 1.0\ \mathrm{A\,cm^{-2}}$ (Toray), (– – –) $i = 0.1\ \mathrm{A\,cm^{-2}}$ (SIGRACET®); (– · · – · · –) $i = 1.0\ \mathrm{A\,cm^{-2}}$ (SIGRACET®).

source. A constant temperature boundary condition is specified on both the backing plate, and temperature and heat flux continuity is imposed on each interface in the domain. Thermal contact resistance is also accounted on the backing plate–diffusion media interface and the value is used from our experimental result. The heat generation in catalyst layer can be written as [42]:

$$q''' = \frac{i}{t_{\mathrm{cl}}}\left[\left(\frac{T\Delta S}{nF}\right) + \eta\right] \tag{5}$$

where n is the number of electrons per mole of the reactants, ΔS the half-cell change in the entropy ($\mathrm{J\,mol^{-1}\,K^{-1}}$), i the current density ($\mathrm{A\,cm^{-2}}$), η the voltage drop (over-potential) due to activation, concentration and ohmic resistance (V), t_{cl} the thickness of the catalyst layer (μm) and F is the Faraday constant. The entropy change at standard state with platinum catalyst is taken as $\Delta S = 0.104\ \mathrm{J\,mol^{-1}\,K}$ for the anode side, and $\Delta S = -326.36\ \mathrm{J\,mol^{-1}\,K^{-1}}$ for the cathode side [43]. The activation over-potential was calculated based on typical Tafel kinetics for a Pt-electrode at the normal operating condition. For the membrane ohmic resistance (Joule heating) is accounted for volumetric heat generation.

Based on Eqs. (4) and (5), a temperature profile in the fuel cell components was obtained and shown in Fig. 11 for two different current densities of 0.1 and $1\ \mathrm{A\,cm^{-2}}$ with SIGRACET® and Toray carbon paper diffusion media. The model parameters are listed in Table 3. For a 200 μm thick diffusion media, 5 wt.% PTFE content SIGRACET® has an almost 3–4 °C drop in the diffusion media as compared to 1–2 °C temperature drop in Toray carbon paper for $i = 1\ \mathrm{A\,cm^{-2}}$. However, temperature is almost uniform for lower current density, i.e. $i = 0.1\ \mathrm{A\,cm^{-2}}$. From the scale analysis, 7–8 °C temperature drop can be expected for 400 μm thick diffusion media at $i = 1.0\ \mathrm{A\,cm^{-2}}$. A temperature drop of 10–12 °C was also measured by Burford and Mench [23], and estimated by Hwang [3] for much thicker diffusion media, and is consistent with the current model results. This temperature drop has a significant affect on the water saturation curve.

Table 3
Geometric and material parameters used in simplified analytical model

Parameter	Value
Membrane thickness	50 μm
Anode/cathode diffusion media thickness	200 μm
Anode/cathode catalyst layer thickness	25 μm
Backing plate thickness	2 mm
Membrane thermal conductivity	$0.12\ \mathrm{W\,m^{-1}\,K^{-1}}$
Membrane ionic conductivity	$8\ \mathrm{S\,m^{-1}}$ [2,4]
Anode/cathode diffusion media thermal conductivity	$1.7\ \mathrm{W\,m^{-1}\,K^{-1}}$ (Toray), $0.31\ \mathrm{W\,m^{-1}\,K^{-1}}$ (SIGRACET® 5 wt.%)
Anode/cathode catalyst layer thermal conductivity	$0.27\ \mathrm{W\,m^{-1}\,K^{-1}}$
Backing plate (BP) thermal conductivity	$55\ \mathrm{W\,m^{-1}\,K^{-1}}$
Thermal contact resistance BP–diffusion media	$2 \times 10^{-4}\ \mathrm{m^2\,K\,W^{-1}}$
Backing plate end temperature	80 °C

All experiments performed in the current work were to measure thermal conductivity in the through-plane direction for fuel cell components. Due to the highly anisotropic nature of porous diffusion media, thermal conductivity in the in-plane direction also plays a very crucial role in the heat transfer in PEFC and will be investigated in future study.

4. Conclusion

An experimental technique, based on the steady state method was used to precisely determine the though-plane thermal conductivity and contact resistance of varying fuel cell components, including the electrolyte, catalyst layer and several types of dif-

fusion media. The following conclusions can be made regarding this work:

(i) Thermal conductivity of dry Nafion® membrane was measured to be $0.16 \pm 0.03\,W\,m^{-1}\,K^{-1}$ at 30 °C, and the extrapolated thermal conductivity at 80 °C was $0.11 \pm 0.02\,W\,m^{-1}\,K^{-1}$, decreases with increase in temperature.

(ii) The effect of humidity on thermal conductivity of the Nafion® membrane was estimated using a volume average technique. The thermal conductivity of Nafion® increases with the water content. For a fully humidified membrane, the thermal conductivity was estimated to be $0.29 \pm 0.03\,W\,m^{-1}\,K^{-1}$ at 65 °C.

(iii) The experimentally measured thermal conductivity for Toray carbon paper was $1.80 \pm 0.27\,W\,m^{-1}\,K^{-1}$ at 26 °C and it decreases with increase in temperature. The tightly compressed thermal contact resistance for Toray carbon paper with smooth aluminium bronze material was estimated as $2.0 \times 10^{-4}\,m^2\,K\,W^{-1}$ at a compression pressure of 2 MPa and over.

(iv) The thermal conductivity of PTFE treated diffusion media decreases with increase in the PTFE content. The thermal conductivity of SIGRACET® untreated (0 wt.%), 5 and 20 wt.% PTFE content diffusion media was measured to be 0.48 ± 0.09, 0.31 ± 0.06 and $0.22 \pm 0.04\,W\,m^{-1}\,K^{-1}$, respectively.

(v) The thermal contact resistance of SIGRACET® diffusion media with aluminium bronze material is almost constant with varying PTFE content and is order of $1.2–1.5 \times 10^{-4}\,m^2\,K\,W^{-1}$ at 2.2 MPa.

(vi) The effective thermal conductivity of a catalyst layer having $0.5\,mg\,cm^{-2}$ platinum on carbon was estimated to be $0.27 \pm 0.05\,W\,m^{-1}\,K^{-1}$.

(vii) A simple one-dimensional analytical model was used to predict the temperature drop of 3–4 °C was estimated for 200 μm thick SIGRACET® 5 wt.% diffusion media at $1\,A\,cm^{-2}$ 80 °C operating condition.

This study should be useful to resolve discrepancies in missing values of thermal conductivity in the literature of various fuel cell materials and help modelers to estimate the temperature distribution in an operating PEFC.

Acknowledgements

This work was partially supported by the Advanced Technology Center, R&D Division for Hynduai Motor Company (HMC) & Kia Motors Corporation (KMC). The authors are thankful to Mr. Suhao He, Mr. Soowhan Kim, Mr. Emin Caglan Kumbur, Ms. Elise Corbin and Mr. Thomas Chorman for their help during the experimentation.

References

[1] H. Ju, H. Meng, C.Y. Wang, Int. J. Heat Mass Transfer 48 (2005) 1303–1315.
[2] T. Berning, D.M. Lu, N. Djilali, Journal of Power Sources 106 (2002) 284–294.
[3] J.J. Hwang, J. Electrochem. Soc. 153 (2) (2006) A216–A224.
[4] E. Birgersson, M. Noponen, M. Vynnycky, J. Electrochem. Soc. 152 (5) (2005) A1021–A1034.
[5] B.D. Washo, D. Hansen, J. Appl. Phys. 40 (8) (1969) 2423–2427.
[6] K. Kurabayashi, Int. J. Thermophys. 22 (1) (2001) 277–288.
[7] Y. Zhang, S. Tadigadapa, Appl. Phys. Lett. 86 (2005) 034101.
[8] K. Kurabayashi, M. Asheghi, M. Touzelbaev, K.E. Goodson, IEEE J. Microelectromech. Syst. 8 (2) (1999) 180–191.
[9] Y.S. Ju, K. Kurabayashi, K.E. Goodson, Thin Solid Films 339 (1999) 160–164.
[10] C.L. Choy, G.W. Yang, Y.W. Wong, J. Polym. Sci.: Polym. Phys. Ed. 35 (1997) 1621–1631.
[11] C.L. Choy, Y.W. Wong, G.W. Yang, T. Kanamoto, J. Polym. Sci.: Polym. Phys. Ed. 37 (1999) 3359–3367.
[12] K. Eiermann, K.H. Hellwege, J. Polym. Sci. 57 (1962) 99–106.
[13] N. Sabte, J. Santander, I. Gracia, L. Fonseca, E. Figueras, E. Cabruja, C. Cane, Thin Solid Films 484 (2005) 328–333.
[14] D. Chu, M. Touzelbaev, K.E. Goodson, S. Babin, R.F. Pease, J. Vac. Sci. Technol. B 19 (6) (2001) 2874–2877.
[15] G. Langer, J. Hartmann, M. Reichling, Rev. Sci. Instrum. 68 (3) (1997) 1510–1513.
[16] C.L. Choy, W.P. Leung, Y.K. Ng, J. Polym. Sci.: Part B Polym. Phys. 25 (1987) 1779–1799.
[17] L. Song, Y. Chen, W. Evans, J. Electrochem. Soc. 144 (11) (1997) 3797–3800.
[18] L. Song, J.W. Evans, J. Electrochem. Soc. 146 (3) (1999) 869–871.
[19] E.E. Morotta, L.S. Fletcher, J. Thermophys. Heat Transfer 10 (2) (1996) 334–342.
[20] J.J. Fuller, E.E. Marotta, J. Thermophys. Heat Transfer 15 (2) (2001) 228–238.
[21] I. Savija, J.R. Culham, M.M. Yovanovich, E.E. Marotta, J. Thermophys. Heat Transfer 17 (1) (2003) 43–52.
[22] P.S. Vie, S. Kjelstrup, Electrochim. Acta 49 (2004) 1069–1077.
[23] D.J. Burford, M.M. Mench, Heat transport and temperature distribution in PEFC, in: Proceeding of the IMECE'04, ASME International Mechanical Engineering Congress and Exposition, Anaheim, CA, 2004.
[24] A. Rowe, X. Li, J. Power Sources 102 (2001) 82–96.
[25] P. Argyropoulos, K. Scott, W.M. Taama, J. Power Sources 79 (1999) 169–183.
[26] V.V. Rao, K. Bapurao, J. Nagaraju, M.V. Krishna Murthy, Meas. Sci. Technol. 15 (2004) 275–278.
[27] F.P. Incropera, D.P. DeWitt, Fundamentals of Heat and Mass Transfer, 4th ed., John Wiley & Sons, 1996.
[28] E.M. Sparrow, in: E.R.G. Eckert, R.J. Goldstein (Eds.), Measurement in Heat Transfer, 2nd ed., Hemisphere Publishing Corporation, Washington, 1976, pp. 1–24.
[29] S.J. Kline, F.A. McClintock, J. Am. Soc. Mech. Eng. 75 (1953) 3–8.
[30] P.C. Powell, Engineering with Polymers, Chapman and Hall, London, 1983.
[31] K.A. Mauritz, R.B. Moore, Chem. Rev. 104 (2004) 4535–4585.
[32] B. Smitha, S. Sridhar, A.A. Khan, J. Membr. Sci. 259 (2005) 10–26.
[33] S. Banerjee, D.E. Curtin, J. Fluorine Chem. 125 (2004) 1211–1216.
[34] W.Y. Hsu, T.D. Gierke, J. Membr. Sci. 13 (3) (1983) 307–326.
[35] T.D. Gierke, G.E. Munn, F.C. Wilson, J. Polym. Sci.: Polym. Phys. Ed. 19 (1981) 1687–1704.
[36] C.L. Choy, S.P. Wong, K. Young, J. Polym. Sci.: Polym. Phys. Ed. 23 (1985) 1495–1504.
[37] Toray carbon paper – Manufacturer data sheet. Web: http://www.torayca.com/index2.html.
[38] SIGRACET® diffusion media, manufacture data sheet. Web: http://www.sglcarbon.com/sgl_t/fuelcell/index.html.
[39] Web: http://carbon.biography.ms/.
[40] Web: http://www.boedeker.com/ptfe_p.htm.

[41] M.F. Mathias, J. Roth, J. Fleming, W. Lehnert, in: W. Vielstich, H.A. Gasteiger, A. Lamm (Eds.), Handbook of Fuel Cells—Fundamental, Technology and Application, vol. 3, John Wiley & Sons, Ltd., 2003, pp. 517–537.
[42] B.R. Sivertsen, N. Djilali, J. Power Sources 141 (2004) 65–78.
[43] M.J. Kampien, M. Fomino, J. Electrochem. Soc. 140 (12) (1993) 3537–3546.